Chapter 3

Carbon Thin Films from Camphor by Ion Beam Sputtering : Optoelectrical and Structural Properties

3.1 Introduction

There is a growing interest in amorphous carbon (a-C) and hydrogenated amorphous carbon (a-C:H) thin films because of their well-known outstanding properties such as chemical inertness, high hardness, high electrical resistivity, high thermal conductivity, high dielectric strength, infrared transparency and band gap varying over a wide range from that of insulating diamond (~5.5 eV) to that of metallic graphite (~0.0 eV). a-C or a-C:H thin films are prepared by various methods such as pulsed laser deposition [1-4], ion beam deposition [5,6], sputtering [7,8], chemical vapor deposition (CVD) [9,10] and r.f./microwave plasma CVD [11-16]. The properties of a-C films strongly depend on the precursor material and method of deposition. Hydrogen in a-C films modifies the properties of the films and introduces many sp^3 sites, causing an increase in the band gap [17]. Depending on the conditions and method of deposition, carbon films containing varying proportions of fourfold (sp^3)- and threefold (sp^2)-coordinated bonded a-C or a-C:H can be obtained. A tetrahedral (sp^3)-coordinated carbon atom has four in-plane σ bonds while a trihedral (sp^2) has three σ bonds and one π orbital normal to the σ -bonded plane. Photon-assisted electronic transitions occur between filled bonding states (σ or π) and the empty anti bonding (σ^* or π^*) states [18]. Since π states are more weakly bonded, they lie closer to the Fermi level (EF) than the σ states. Therefore, filled π states form valence band edges while

empty π^* states form conduction band edges, and these (π and π^*) states control the size of the optical gap. Electronic properties are also controlled by these lower-gap bands. Therefore, the optical and electrical properties of these films are of much interest because of their potential application in semiconductor technologies including photonic devices. Studies of optoelectrical properties of carbonaceous thin films are in progress. A wide range of absorption characteristics is observed depending on the deposition method. Although the electrical conductivity of a-C and a-C:H has been studied by many workers [10, 16, 18-20], there is no generally accepted explanation of the conduction mechanism due to the high density of localized states in shallow and deep states of amorphous films. a-C films have more complexity due to the presence of π and π^* states.

To our knowledge, so far, graphite is commonly used as a target material in sputtering and arc deposition methods for the preparation of a-C thin films. However, camphor ($C_{10}H_{16}O$), a natural source, is a new precursor material thought to have an additional advantage over graphite in the sense that while the latter is purely sp^2-hybridized, the former consists of both sp^2- and sp^3-hybridized carbons in its structure. Camphor has already been used as a precursor material, to generate various forms of carbon such as fullerenes [21], multichannel-multilayered micro/nanotubules [22] semiconducting carbon [23] and diamond-like carbon (DLC) [24] for their application in light energy conversion devices [25]. Recently, nanodiamonds have also been produced from camphor by pyrolysis [26]. Here, we report the detailed optical and electrical properties of ion-beam-sputtered amorphous camphoric carbon (a-CC) thin films. Effects of heat treatment on absorption and electrical conduction characteristics are discussed and compared. The electrical conduction mechanism in camphoric carbon thin films is also outlined for the first time.

3. 2 Experimental Details

3.2.1 Preparation of Thin Films

3.2.1.1 Target Preparation

Camphor has been used as a source of carbonaceous thin film. The chemical structure of a camphor molecule is shown in Fig.1.1. Camphor was burnt in a 1-metre-long and 11-cm-diameter quartz tube. A schematic representation of the experimental setup constructed for the generation of carbon soot by burning camphor is shown in Fig. 3.1. The soot deposited along the walls of the tube was collected, dried in the oven for an hour and pressed into pellets. These pellets were used as targets for carbonaceous thin films by ion beam sputtering.

3.2.1.2 Thin Film Deposition

Sputtering of the a-CC was carried out in an argon discharge at a base pressure of 2×10^{-6} Torr. Quartz and single-crystal silicon substrates were used for deposition at room temperature. Before deposition, substrates were cleaned with acetone and methanol in a hot water bath at 55℃ for 5 min each. After cleaning, they were etched with HF:H_2O (1:10 ratio) in order to remove the resistive native oxide formed over the surface, and quickly transferred into the deposition chamber. Substrates were placed on a rotating holder at 4 rev/min to obtain uniform films. The target was sputtered for 15 min prior to film deposition in order to remove the dust and oxygen adsorbed over the top few layers. Sputter power of 20W (1KV, 20mA) was used for film deposition. Films were heat treated at 200℃, 400℃, 600℃ and 800℃ in nitrogen atmosphere for 10 min.

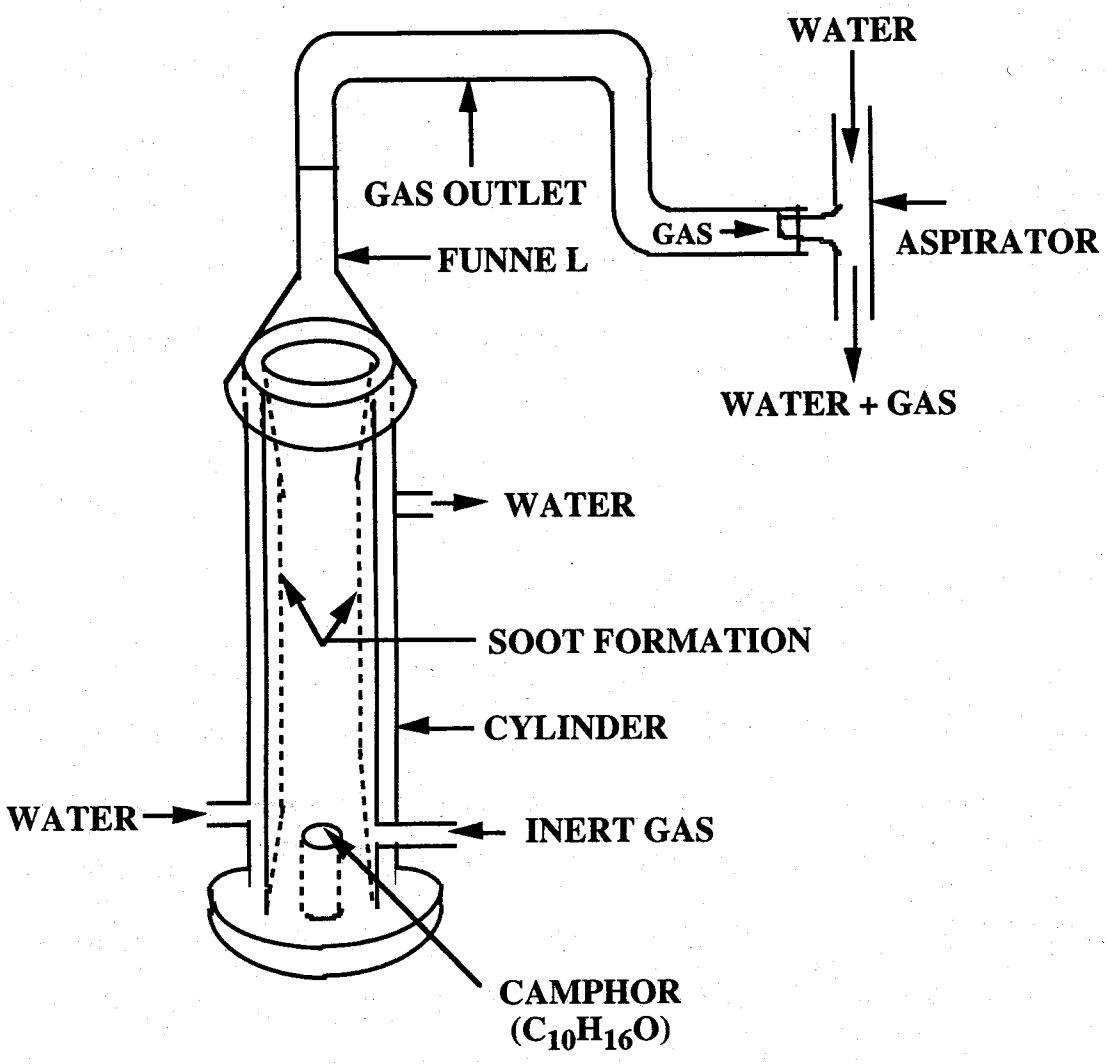

Figure 3.1. Schematic representation of the camphor burning system.

3.3 Characterization of Films

3.3.1 Optical and Electrical Properties

The optical and electrical characterizations were carried out using the films deposited on quartz substrates. As-deposited and heat treated films were studied for their optical and electrical properties. Optical properties of the films were investigated by spectral transmittance and reflectance measurements in the range of 350~1150 nm. The Tektronix VX1410 IntelliFrame from Sony was used for I-V measurement, and temperature of the chamber was maintained by a Cryomini compressor from Iwatani Plantech. Electron-beam-evaporated gold electrodes were used in a gap cell configuration and silver paste was used as a point contact on gold electrodes for conductivity measurements. The electrical conductivity of a-CC films were measured as a function of temperature between 40K and 400K and observed to be linear in the range of our measurement conditions. Depending on the conductivity of the samples at different temperatures, 100 mV to 20 V supply was used.

3.3.1.1 Results

From the measurements of optical reflectance and transmittance in the range of 300 to 1150nm wavelength, an optical absorption coefficient (α) on the order of 10^4-10^5 cm^{-1} is obtained. The energy ($h\nu$) dependence of the optical absorption coefficient is shown in Fig. 3.2. Optical absorption edges of these carbon films are broad and increase upon heat treatment. In Fig. 3.3, a plot of $(\alpha h\nu)^{1/2}$ versus $h\nu$ is shown using the relation [27]

$$(\alpha h\nu)^{\frac{1}{2}} = B(E_{opt} - h\nu) \tag{3.1}$$

where, B is the density of the localized state constant and E_{opt} is the optical gap obtained from the extrapolation of the linear part of the curve at the absorption coefficient α=0. The change of the optical gap as a function of heat treatment temperature (HTT) is shown in Fig. 3.4. The optical gap of as-deposited camphoric carbon film is 0.5 eV which is typical for sputtered

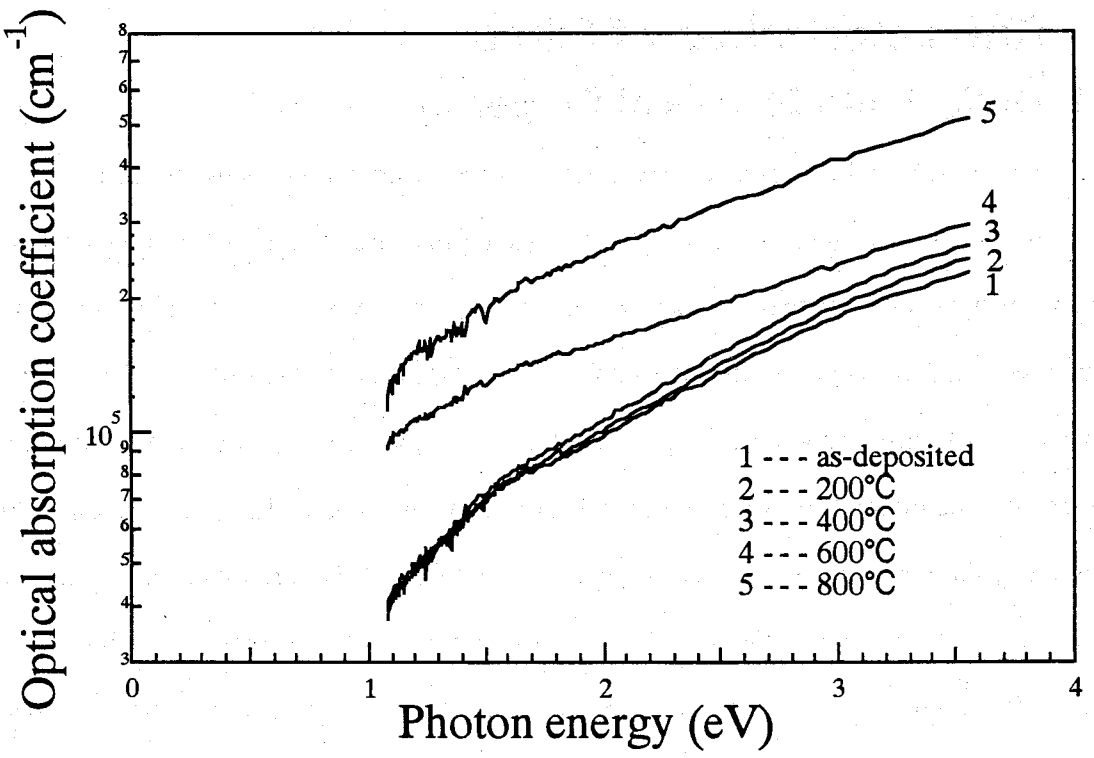

Figure 3.2. Optical absorption coefficient (α) plotted as a function of photon energy ($h\nu$), for as-deposited and heat treated camphoric carbon thin films.

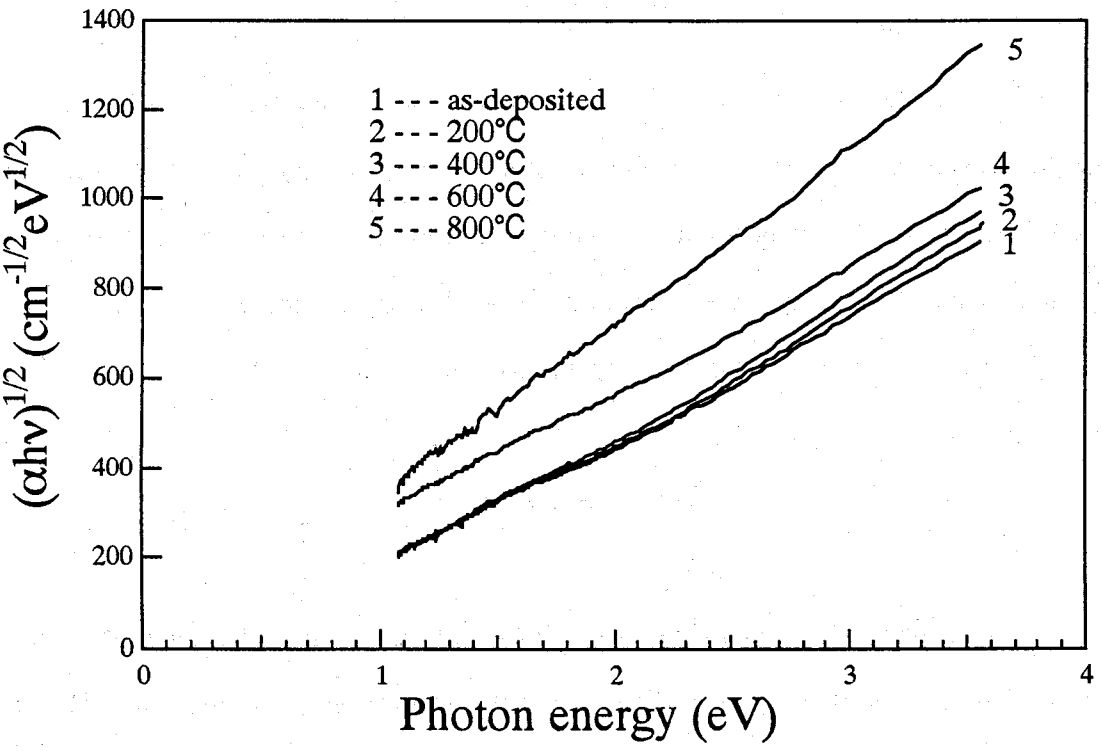

Figure 3.3. $(\alpha h\nu)^{1/2}$ as a function of photon energy plotted for as-deposited and heat treated a-CC thin films.

carbon films [8,19,28]. The optical gap remains almost constant up to 400℃ and decreases rapidly at higher HTTs.

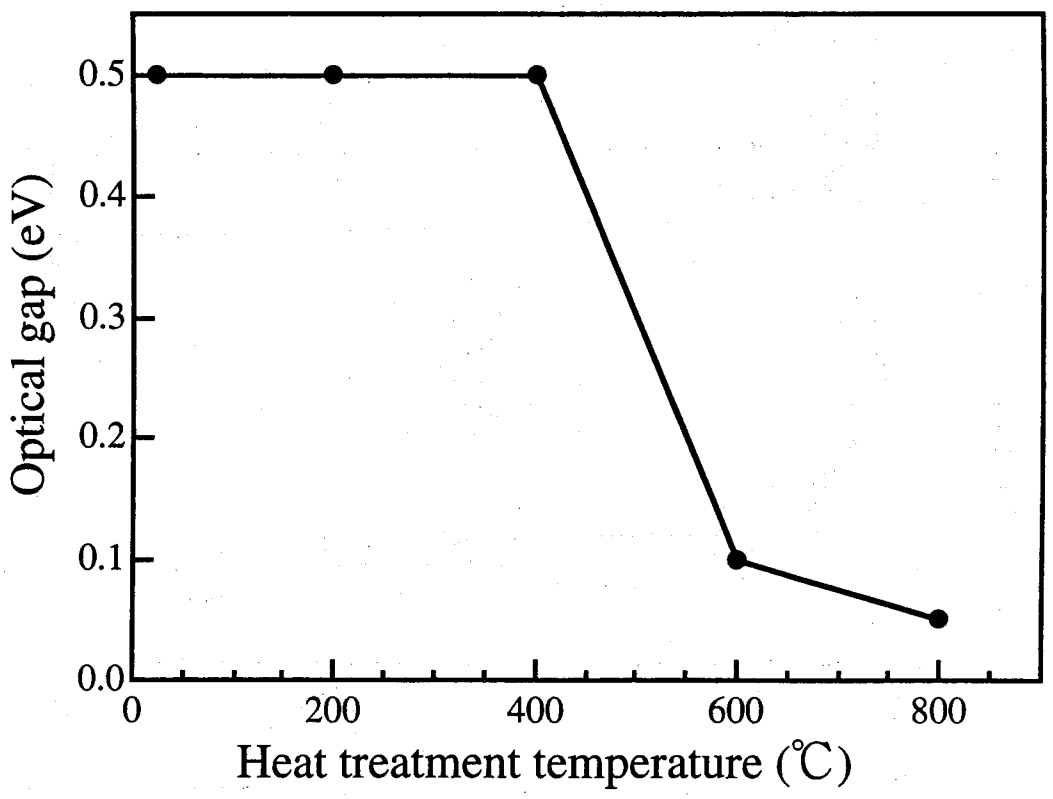

Figure 3.4. A plot of optical gap of a-CC thin films as a function of heat treatment temperature.

The results of electrical conductivity measurement of carbon films are shown in Fig. 3.5, where conductivity σ(T) is plotted against inverse temperature on a logarithmic scale. Conductivity is found to increase with the measurement temperature for both as deposited and HT films. No permanent change in conductivity is observed before and after measurement. The conductivity plot in Fig. 3.5 does not follow the simple activated form

$$\sigma(T) = \sigma_{01} \exp(-E_a / KT) \tag{3.2}$$

where σ_{01} is the conductivity pre factor, T is the absolute temperature, K is Boltzmann's constant and E_a is the activation energy with respect to the Fermi level.

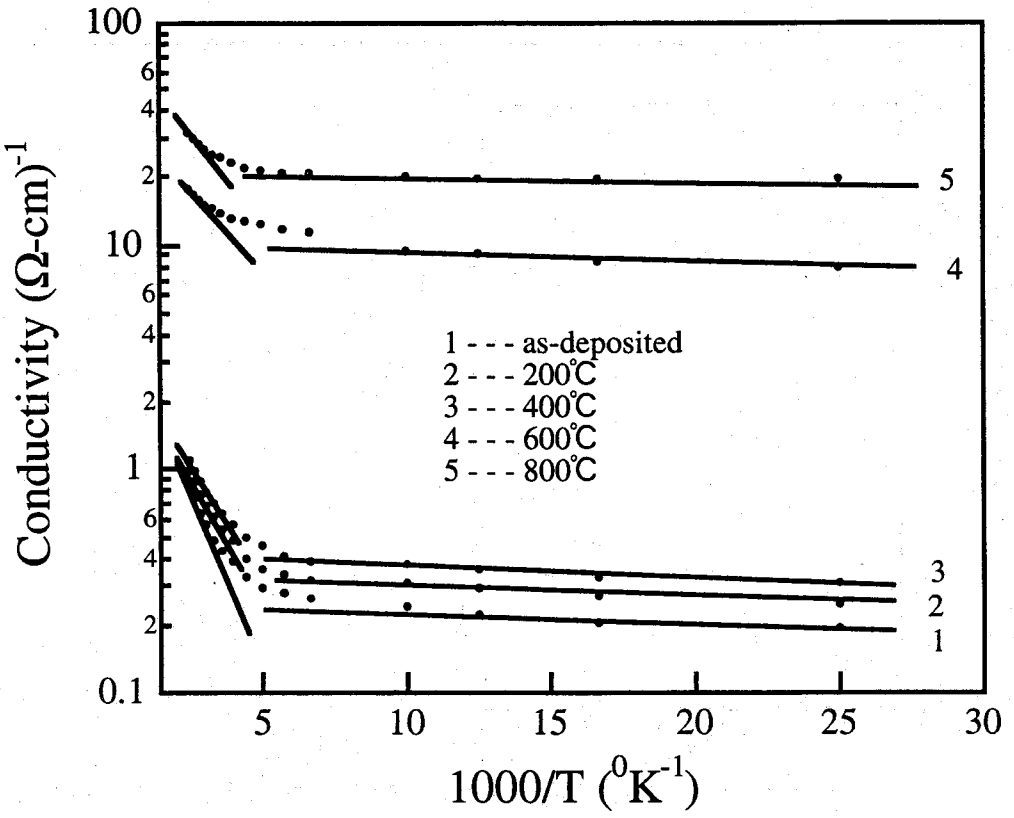

Figure 3.5. Temperature dependence of conductivity of camphoric carbon thin films as a function of T^{-1}.

Conductivity σ(T) is also plotted as a function of $T^{-1/4}$ on a logarithmic scale in Fig. 3.6, according to the Davis and Mott [29] model using the relation

$$\sigma(T) = \sigma_{03} \exp(-(T_{03}/T)^{1/4}) \tag{3.3a}$$

where

$$T_{03} = 16a^3 / KN(E_F) \tag{3.3b}$$

a^{-1} is the radius of the localized states wave function and $N(E_F)$ is the density of localized

states. Here, prefactors σ_{03} and T_{03} are independent of measuring temperature (subscript 03 refers to the 3-dimensional structure of the carbon films).

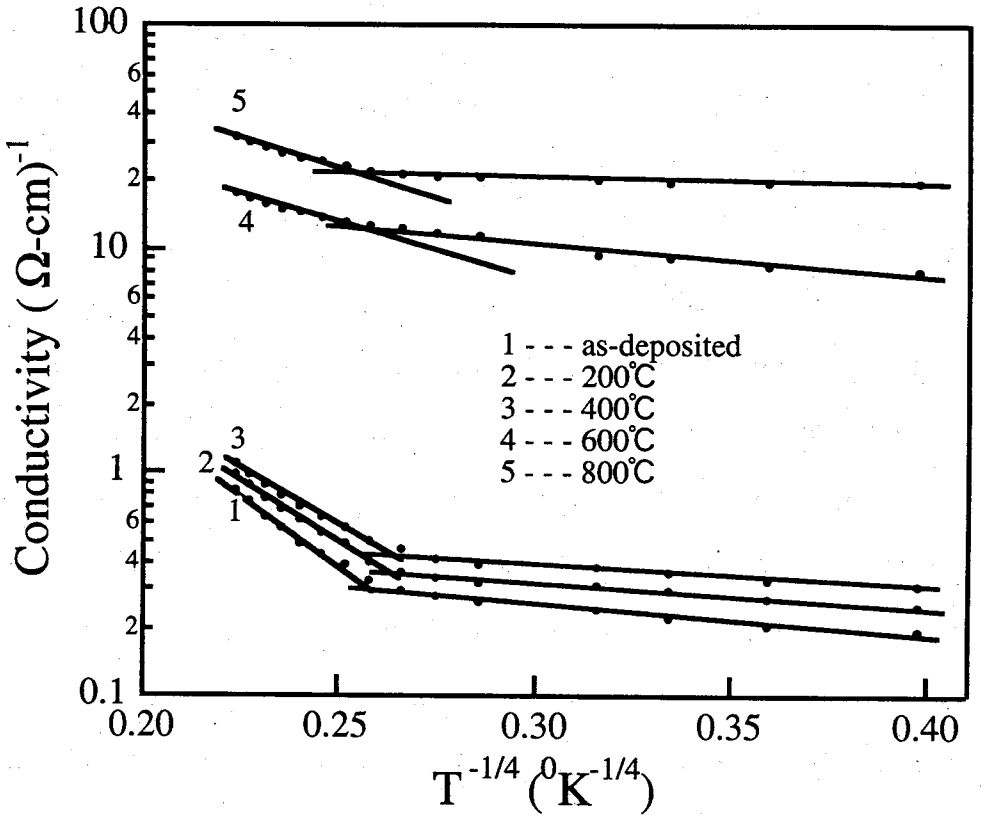

Figure 3.6. Temperature dependence of conductivity of camphoric carbon thin films as a function of $T^{-1/4}$.

Figure 3.6 shows two linear regions in the temperature ranges of 400K≧T >200K and 200K≧T ≧40K which indicate domination of the hopping conductivity of the films. The temperature dependence of the activation energy $E_a(T)$ can be defined by [30,31] $E_a(T)= -K\{ d[\ln \sigma(T)] / d(1/T)\}$ for films that do not follow the simple activated form (Eqn 3.2). Since a linear region is not observed for any particular range of temperature (Fig. 3.5), activation energies [$E_a(T)$] are determined from the slope of the straight parts of logarithmic conductivity curves plotted as a function of inverse temperature (Fig. 3.5) from the highest

temperature side [32] of the two temperature regions (400K≧T >200K and 200K≧T ≧ 40K). The conductivity prefactors [$\sigma_{01}(T)$] are obtained from the extrapolation of the same straight lines with the conductivity axis at 1/T = 0. These data are presented in Tables 3.1 and 3.2. Furthermore, the activation energy obtained for a higher temperature region (400K≧ T>200K) is plotted as a function of HTT in Fig. 3.7. Room-temperature conductivity (σ_{RT}) as a function of HTT is shown in Fig. 3.8. No significant change in conductivity is observed up to 400℃, while a sharp increase is seen above 400℃.

3.3.1.2 Discussions

The optical absorption coefficient of camphoric carbon is found to be similar to those of other forms of sputtered amorphous carbon [8]. A broad optical edge is observed (Fig. 3.2) due to the presence of localized states in the mobility gap. Absorption coefficient a increases slowly up to 400℃, and the increment is higher for higher HTTs. A similar trend can clearly be seen in Fig. 3.3 where $(\alpha h\nu)^{1/2}$ is plotted against the photon energy. The optical gap is almost constant up to 400℃ and a sudden decrease is observed for the films heat treated at higher temperatures (Fig. 3.4). From 400℃ to 600℃, the gradient of the optical gap is 2 meV/K with a negative sign (Fig. 3.4). At 800℃, the optical gap of the carbon film almost vanishes (0.05eV). The optical absorption of the films indicates changes in the bonding and band structure. Upon HT, the films become more graphitic in nature [11,33]. The electrical conductivity of all the films increases with increasing measurement temperatures because of their semiconducting nature. The change of conductivity with measuring temperature, $d\sigma/dT$, decreases for the films heat treated at high temperatures (Fig. 3.5). This characteristic of conductivity is mainly due to the decrease of its optical gap upon HT, as shown in Fig. 3.4.

Table 3.1

Activation energy [$E_a(T)$] and conductivit prefactor [$\sigma_{01}(T)$] of as-deposited and heat treated a-CC films calculated at the highest temperature side of the $400K \geqq T > 200K$ region.

Heat treatment temperature (℃)	Activation energy (meV)	Conductivity prefactors (σ_{01}) $(\Omega\text{-cm})^{-1}$
as-deposited	70	6.36
200	64	6.05
400	58	5.61
600	29	41.25
800	28	70.83

Table 3.2

Activation energy ($E_a(T)$) and conductivity prefactor ($\sigma_{01}(T)$) of as-deposited and heat treated a-CC films calculated at the highest temperature side of the $200K \geqq T \geqq 40K$ region

Heat treatment Temperature (℃)	Activation energy (meV)	Conductivity prefactors (σ_{01}) $(\Omega\text{-cm})^{-1}$
as-deposited	6.4	.43
200	6.1	.53
400	6.0	.87
600	4.0	15.74
800	2.1	28.50

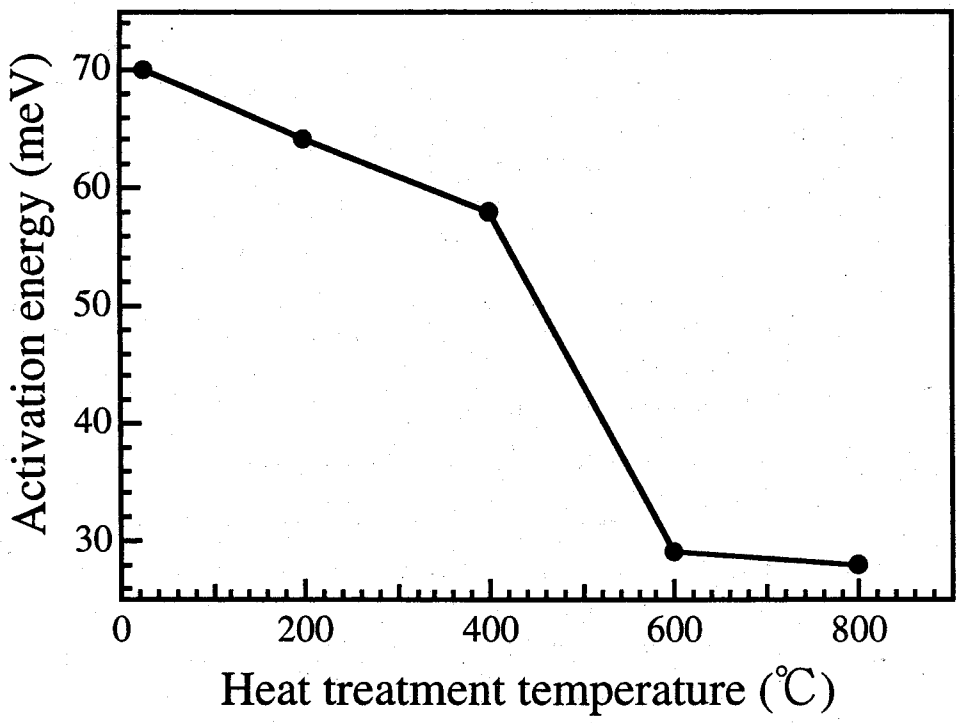

Figure 3.7. A plot of activation energy of a-CC thin films as a function of heat treatment temperature.

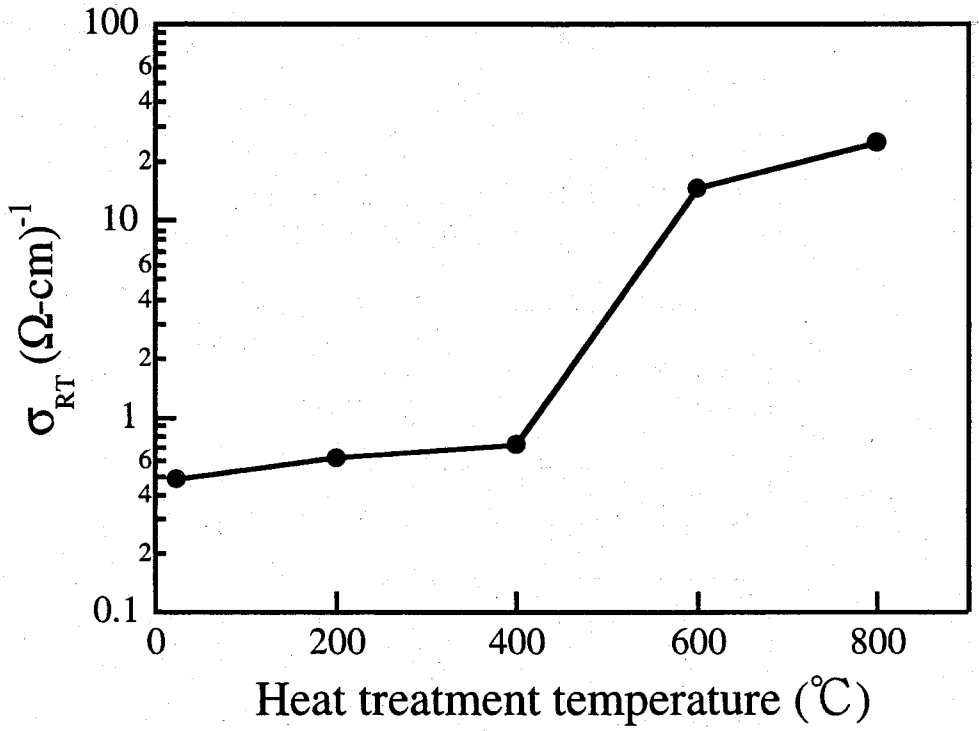

Figure 3.8. Room-temperature conductivity (σ_{RT}) of a-CC thin films as a function of heat treatment temperature.

There is a similarity between the activation energy [$E_a(T)$], conductivity prefactor [$\sigma_{01}(T)$] and room-temperature conductivity (σ_{RT}). The conductivity prefactor and room-temperature conductivity increase suddenly above 400℃ while there is a sharp decrease in activation energy (see Tables 3.1 and 3.2, Figs. 3.7 and 3.8). From Figs. 3.5 and 3.6 and considering the activation energy, conductivity prefactor and room-temperature conductivity values, a similarity in the conductivity mechanism can be inferred between as-deposited, 200℃, and 400℃ heat treated films, and between 600℃ and 800℃ heat treated films. Therefore, to make it easier to visualize the conduction mechanism, the films are divided into two groups.

3.3.1.2.1 Films As-Deposited and Heat Treated up to 400℃

These films have room-temperature conductivity on the order of 10^{-1} $(\Omega\text{-cm})^{-1}$. The optical gap of these films is about 0.5 eV (Fig. 3.4). Activation energies of these films are found to be 58~70 meV for the high-temperature region (400 K≧T >200 K) and 6.4~6.0 meV for the low-temperature region (200 K≧T ≧40 K), measured from the slopes of the highest temperature side of the straight lines, and corresponding conductivity prefactor values are on the order of 100 $(\Omega\text{-cm})^{-1}$ and 10^{-1} (Ω-cm)-1, respectively. Since the films are undoped, the Fermi level (EF) is expected to be near the middle of the mobility edges [34]. Also, at high temperatures, E_F will be in the middle of the forbidden gap. Therefore, in these films, the expected Fermi level position is about 0.25 eV below the conduction band edge. At high temperatures, the activation energy of these films is about 65 meV, i.e., $E_a(T) << E_{opt}/2$, and the conductivity prefactor [~100 $(\Omega\text{-cm})^{-1}$] indicates that conduction is not in the extended states. An extended state conduction requires conductivity prefactor values near 10^3 $(\Omega\text{-cm})^{-1}$ [7]. Assuming a=10, [28] the density of localized states, estimated from data in Fig.3.6 (using Eq. (3.3)), is in the range of 10^{19} to 10^{20} $eV^{-1}cm^{-3}$, which is in agreement with that reported by others [19, 28,35]. Therefore, our results suggest that the possible conduction mechanism in the high-temperature range, i. e., 400 K≧T >200 K, is thermally activated hopping in the tail states. At lower temperatures, when the activation energy becomes much

less than the forbidden gap, variable-range hopping should be observed [36] as is the case in our samples, as detailed below. The activation energy of these films obtained in the low-temperature region, i.e., 200 K≧T ≧40 K, is about 6 meV and the conductivity prefactor is in the range of 10^{-1} $(\Omega\text{-cm})^{-1}$, which are quite low compared to those obtained in the high-temperature region. These values, along with the plots for the lower temperature region in Fig. 3.6, suggest that the possible conduction mechanism in this region is dominated by variable-range hopping conductivity near the Fermi level.

3.3.1.2.2 Films Heat Treated Above 400℃

These films are highly conductive [~10^{1} $(\Omega\text{-cm})^{-1}$] with almost zero optical gap (Fig. 3.4). The gradient of the conductivity is very low [0.04 $(\Omega\text{-cm})^{-1}$/K to 0.06 $(\Omega\text{-cm})^{-1}$/K], which indicates the presence of a high percentage of sp^2 bonds in these films. Because of the vanishing optical gap, the behavior cannot be explained by any semiconductor model.

Plots of optical absorption coefficient α (Fig.3.2), optical gap (Figs.3.3 and 3.4), activation energy $E_a(T)$ (Fig. 3.7) and room-temperature conductivity σ_{RT} (Fig. 3.8) show stable characteristics up to 400℃, while a rapid change is observed thereafter. The change in optical and electrical properties above 400℃ is due to the fundamental changes in the bonding and band structure of the carbon films. The details on the bonding and structural changes upon HT are discussed elsewhere more elaborately through in depth Raman scattering analyses [33]. These characteristics resemble the properties of a-C:H films previously studied by others [11,17,37] and therefore, indicate the presence of hydrogen in our as-deposited camphoric carbon film. We have yet to confirm this by direct measurements of hydrogen concentration. However, the possible explanation for the presence of hydrogen in our films, obtained without using any hydrogen gas source during the deposition, can be derived from the structural properties of our precursor material, camphor which differs from other precursor materials in the sense that it has a large amount of hydrogen in its structure ($C_{10}H_{16}O$, Fig. 1.1). Also, it is reported that at HTTs above 400℃, the hydrogen in the film effuses and hydrogen-bonded

sp^3 carbon converts to C=C-bonded sp^2 carbon [11] which in turn affects various optoelectrical properties of carbon thin films, as seen in our films at 600 and 800 ℃.

3.3.1.3 Conclusions

The summary of these optoelectrical investigations is as follows.

1) The optoelectrical characteristics of carbon thin films deposited by ion beam sputtering of a camphoric carbon target without using any H_2 gas precursor are observed to be similar to those of the hydrogenated a-C films.

2) The optical absorption coefficient of as-deposited film is on the order of 10^4-10^5 cm^{-1} and its optical gap is about 0.5 eV.

3) The optical and electrical properties of these films are almost stable up to 400℃, while abrupt changes are observed at T_a>400℃.

4) The room-temperature conductivity of as-deposited film is on the order of 10^{-1} $(\Omega\text{-cm})^{-1}$, and upon heat treatment up to 800℃, it shows a graphitic nature and the conductivity is increased and reached of the order of 10^1 $(\Omega\text{-cm})^{-1}$.

5) Conductivity is observed not to follow the simple activated form. The conduction mechanism in films as-deposited and heat treated up to 400℃ is dominated by thermally activated hopping in the tail states in the high-temperature region (400 K≧T >200 K), and variable-range hopping near the Fermi level in the low-temperature region (200 K≧T ≧40 K).

Based on these observations, we suggest that precursors similar to camphor, in the sense that they contain both sp^2- and sp^3- bonded carbon in their structure, may be better-suited candidates as starting materials for semiconducting carbon for electronic application. Also, camphor has the additional advantage that it can be used as a precursor in both physical and chemical vapor depositions. More detailed study of these films through in depth Raman scattering measurements are discussed in the following section.

3.3.2 Structural Properties (Raman Investigations)

Amorphous carbon (a-C) thin films have wide range of structural configurations from tetrahedral (sp^3) dominated diamondlike to trihedral (sp^2) dominated graphitelike depending on their method of deposition. Raman spectra (RS) provide a wide range of structural and phase disorder information [38]. There are various forms of carbon [39] and Raman scattering is used as a powerful technique to understand their microstructural changes [40-48]. RS of the two crystalline forms of carbon, graphite and diamond are well known. The first order RS consists of a single line at 1332 cm^{-1} for diamond[49], and 1580 ($\pm$5) cm^{-1} for single crystal graphite [46, 50]. The latter is known as "G" line results from the Raman allowed E_{2g} mode [51] while another line appears also at about 1355 cm^{-1} for polycrystalline graphite, known as "D" line which is due to the breakdown of the k vector conservation rule of the disordered lattice [52]. In general, these two "G" and "D" lines are the most used lines in RS to characterize the carbon materials.

Production of fullerenes [21], multichannel-multilayered micro/nano tubules [23], semiconducting carbon [22], and others [24,26,53] from camphoric carbon (the carbon soot obtained by burning camphor) prompt camphor as a new promising carbon precursor mainly due to its structural advantages [23]. Application in light energy conversion devices, such as photovoltaic solar cell [25, 54] is also reported using amorphous camphoric carbon thin films. However, detailed structural properties of camphoric carbon films have not been reported so far. Effect of heat treatment on the microstructural changes in camphoric carbon films will be useful to study in order to understand the thermal stability of the films for various practical applications. This report is mainly focused on RS of as deposited as well as heat treated ion beam sputtered amorphous carbon films deposited from camphoric carbon soot. Systematic variations of microstructure and optical properties upon heat treatment (HT) studied through Raman scattering, uv-visible and x-ray photoelectron spectroscopies are presented in this section.

The films deposited on silicon substrates were used for Raman and x-ray photoelectron spectroscopy (XPS) studies. To investigate the temperature dependence of microstructure and optical properties, samples were heat treated at different temperatures ranging from 200 to 800 ℃ in nitrogen ambient for 10 minutes. RS were obtained at room ambient conditions in the quasi-backscattering geometry using 488 nm line of Ar^+ laser operating at a power of 200 mW while at the sample it was about 5 mW. The scattered light was analyzed by a double monochromator and detected by a photomultiplier tube. The spectral resolution was 4 cm^{-1} and the films were scanned 3 times at room temperature. The C (1s) core level photoelectron spectra were measured, using an AlKα (hν =1486.6 eV) radiation as an x-ray source, under high vacuum conditions of ~ 10^{-10} torr, to evaluate the tetrahedral to trihedral fraction (sp^3/sp^2) of the carbon bonding [25, 55] present in the films.

3.3.2.1 Results and Discussions

Raman scattering analyses reveal amorphous nature of the carbon and growth of nanocrystallinity upon HT. Figure 3.9 shows RS of the as-deposited and heat treated carbon thin films in the range of 1000 to 1700 cm^{-1}. It is clear that the broad band (peaked at around 1545 cm^{-1}) resulted from the as-deposited film gradually splitted into two peaks (commonly known as D and G lines) due to progressive crystallization upon HT. The spectrum is similar to those observed by Dillon et al. [46]. The typical Raman spectrum of the as-deposited film reveals amorphous nature of the camphoric carbon. The experimental data were best fitted (accuracy factor ~ 0.95) by two peaks considering Gaussian line shapes and linear. The peak position, peak width and the integrated intensity of the two peaks are obtained from the fittings.

Figure 3.10 shows the shift of the G line from about 1545 to 1590 cm^{-1}, indicates the formation of disordered nanocrystalline graphitic particles, upon HT. Up to 600℃ heat treatment temperature (HTT), the upward shift occurs rapidly and remain almost constant

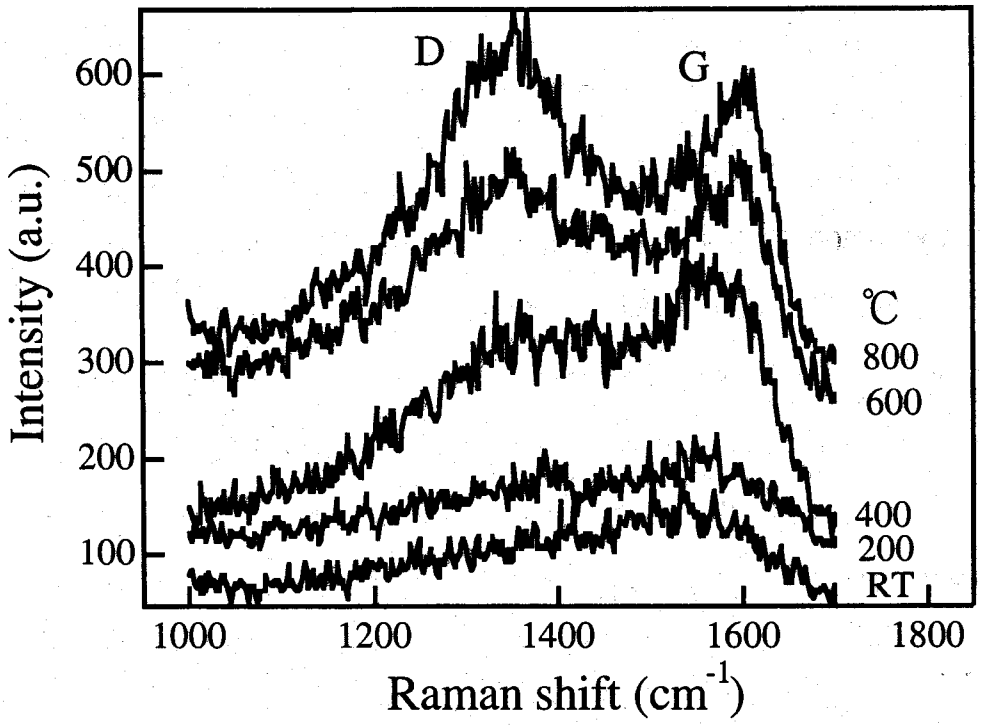

Figure 3.9. Raman spectra of as-deposited (RT) and heat treated carbon thin films.

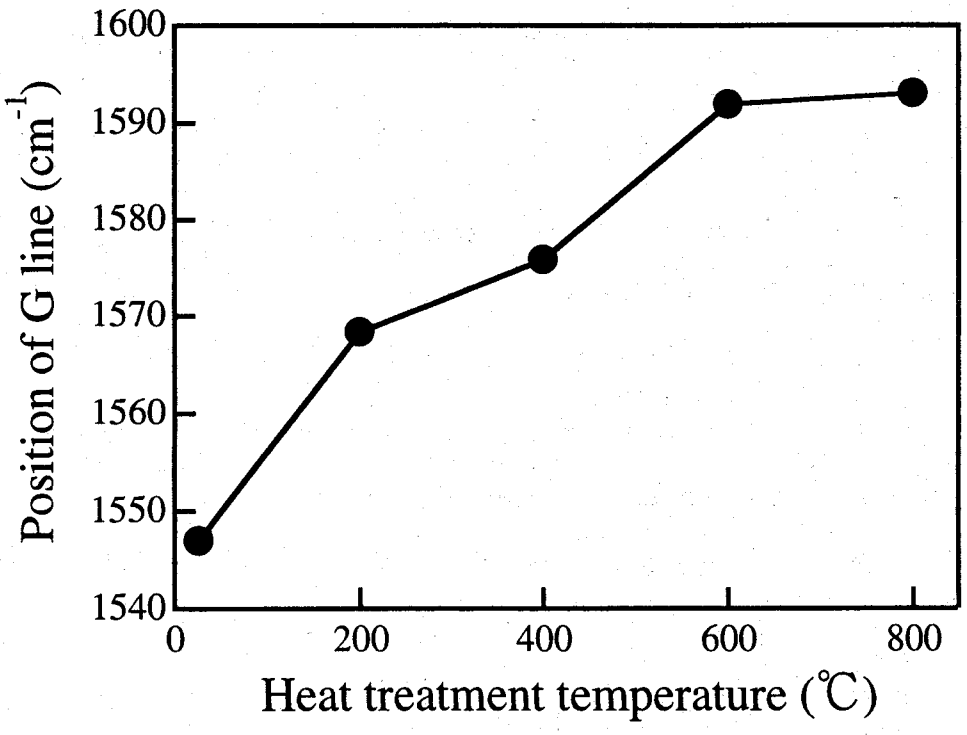

Figure 3.10. Dependence of Raman G line position on heat treatment temperature.

thereafter which means that the saturation of the G line position has taken place. The upshift of G line towards higher frequency (above 1580±5 cm^{-1}) implies that the films heat treated at high temperatures (>400℃) are dominated by trihedral bonding rather than tetrahedral bonding and the crystallites have a very small grain size [56]. This trend is similar to the observation made by Dillon et al. [46]. The shift of the D line as a function of HTT is shown in Fig. 3.11.

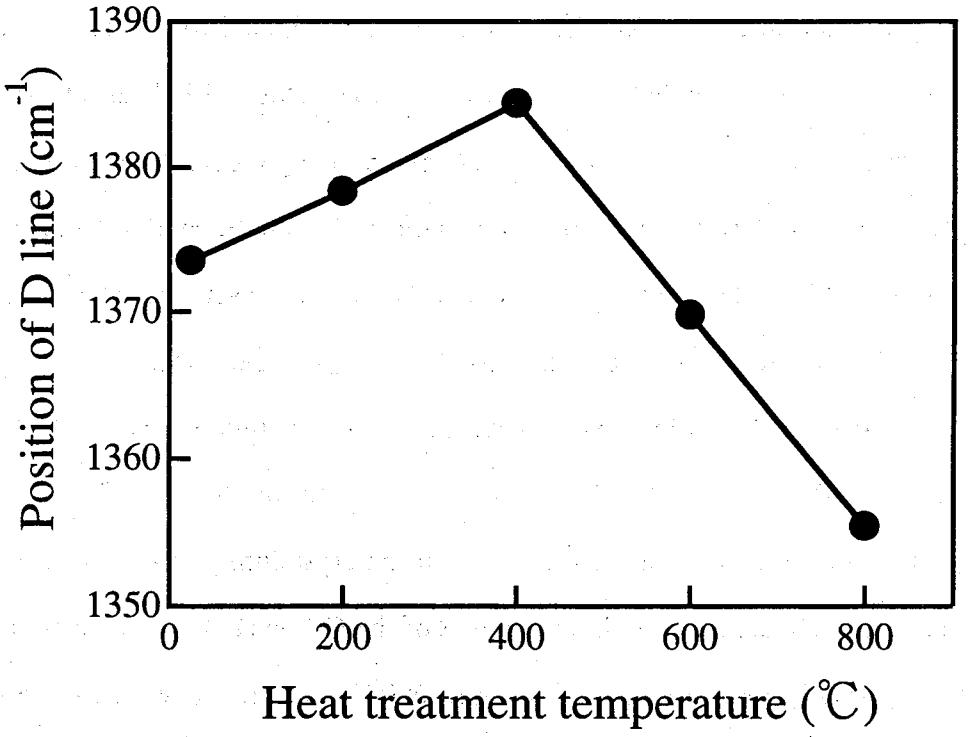

Figure 3.11. Dependence of Raman D line position on heat treatment temperature.

It was observed that while the position of G line maintains below 1575 cm^{-1}, the D line shifts towards higher wave number and was related with the typical amorphous nature of the carbon films [57]. Our films also follow such trend (see Figs. 3.10 and 3.11) and moreover, as an interesting observation, the D line shift is quite different from the RS of a-C thin films which were reported by others. Richter et al. [58] observed an upshift of D line up to a certain value of the substrate bias where after it shifts down but much explanation was not made for such

behavior. Dillon et al. observed an upshift of D line as a function of annealing temperature up to 400℃ which remained almost constant thereafter. However, we observed a transition in the D line from upward direction to downward direction at about 400℃ HTT. The position of D line of as-deposited carbon film is 1374 cm^{-1} which shifts upward to 1385 cm^{-1} at 400℃ HTT and sudden change in shift to downward is observed at elevated HTTs. According to our observations, upshift of D line in carbon films upon HT is due to the change of bond-angle disorder up to 400℃ HTT and downshift at high HTTs is due to the change in bonding (sp^3/sp^2) which in turn affects the structure of the films. From Figs. 3.10 and 3.11, the shift of the two lines from their respective principle values (1580 and 1355 cm^{-1}) of crystalline graphite phase indicate the presence of the bond-angle disorder [56]. Furthermore, the downshift of the G line from 1580 cm^{-1} does indicate the presence of sp^3 bonds which is confirmed through XPS analysis. The shift of G and D lines are discussed later in more detail with respect to HT dependence of optical gap and sp^3 fraction of the films.

The variation of the widths, the full width at half maximum (FWHM), of D and G lines as a function of HTT are shown in Fig. 3.12. It is clear that the FWHM decreases significantly upon HT which indicates the increase of the crystallinity [59]. Figure 3.13 shows the ratio of the integrated areas of the D line to that of the G line (I_D/I_G) as a function of HTT. The I_D/I_G ratio gradually increases upon HT (upto 600℃) and decreases thereafter. It was reported [60] that the intensity of the D line has a limiting value and is restricted by the density of states in the region of the K point, and our results are in good agreement with those interpretations. Increase of I_D/I_G ratio (Fig. 3.13) along with decrease of peak widths of both G and D lines (Fig. 3.13) with increasing HTTs indicate growth of crystallites and removal of the bond-angle disorder. Dorfman et al. [59] have also observed similar behaviour for their films heat treated at 450℃.

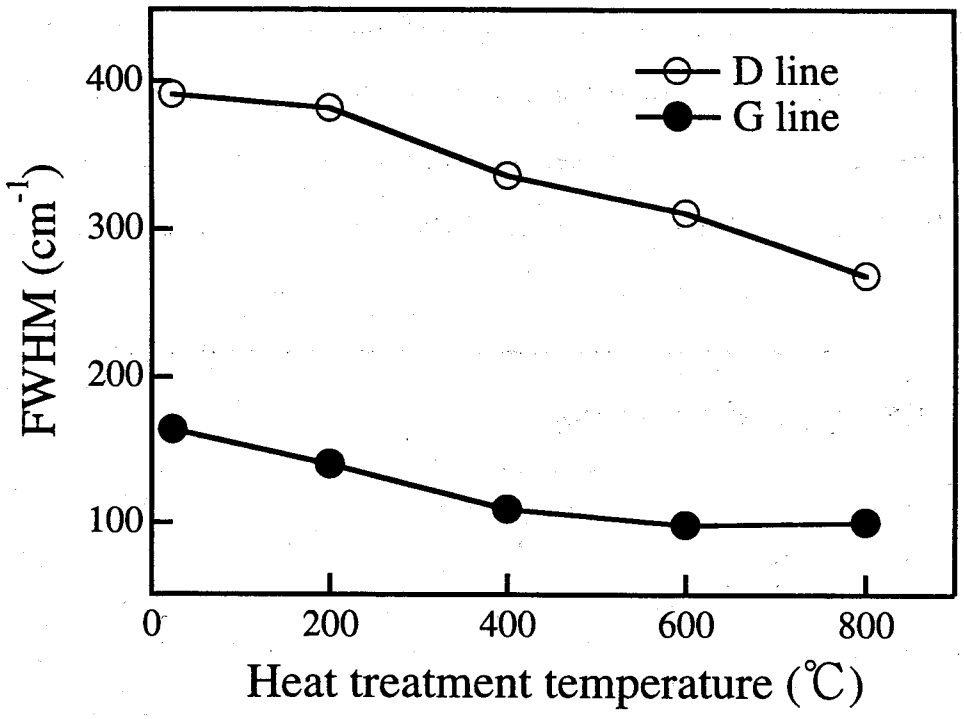

Figure 3.12. Plots of the Raman G and D line width (FWHM) Vs heat treatment temperature.

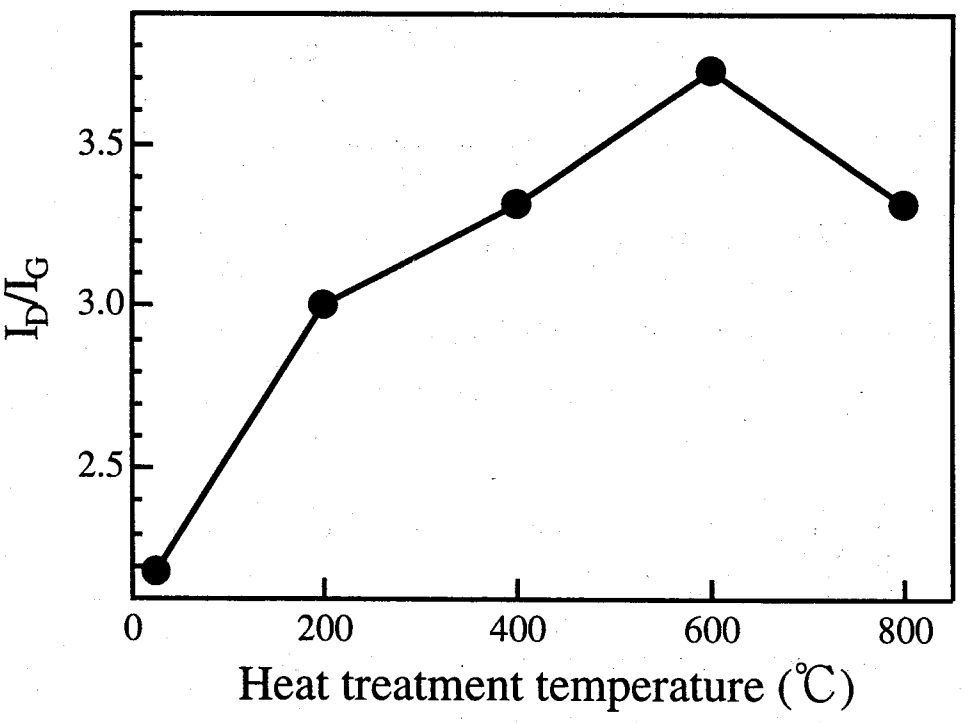

Figure 3.13. Ratio of the integrated areas of the Raman D and G lines (I_D/I_G) as a function of heat treatment temperature.

It is also reported that I_D/I_G ratio starts to decrease with the increase of the crystallites at high HTTs [46] which is the case in our heat treated (≧600℃) samples. Using the inverse relationship [38] between the crystallite size (L_a) and I_D/I_G ratio, we have obtained L_a of 12 and 14 Å for 600 and 800 ℃ heat treated films, respectively. These results are in good agreement with Dillon et al. [46] where they have observed 16 Å for their film heat treated at 800℃.

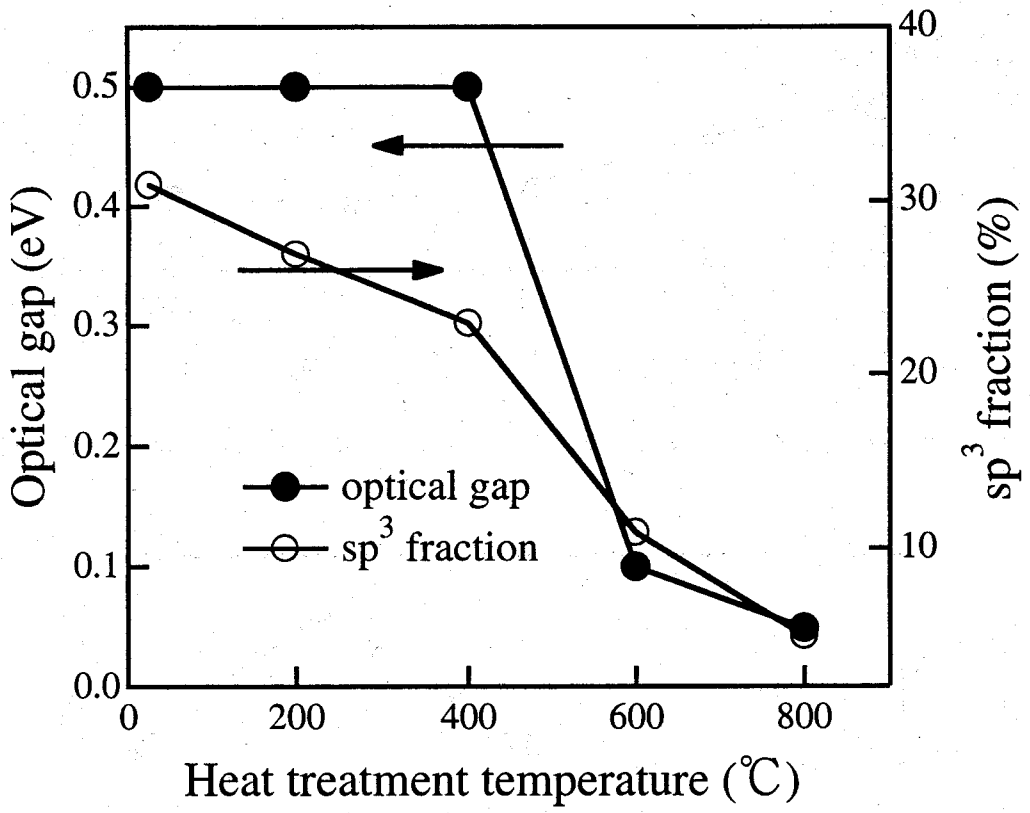

Figure 3.14. Plots of optical gap (left axis) and sp^3 fraction (right axis) as a function of heat treatment temperature.

HTT dependence of optical gap (left axis) and sp^3 fraction (right axis) are shown in Fig. 3.14. It is observed that the optical gap is almost constant and sp^3 fraction changes a little upto 400℃ while both decrease rapidly at higher HTTs. Also, it is known [11,17,37] that hydrogen in carbon films evolves at higher HTTs, thereby plays a vital role for structural changes, such as, fraction of sp^3 bonded carbons. Electrical properties of the same set of films

also observed to show similar transition at 400℃ HTT (details are discussed in terms of the presence of hydrogen in as-deposited camphoric carbon films, in previous section (see Sec. 3.3.1). Optical gap is almost unchanged and sp^3 fraction decreases slowly upto 400℃ (Fig. 3.14) and thereafter both decrease sharply while upshift of G line is observed up to the saturation value of about 1590 cm^{-1} (Fig. 3.10). These results support the theoretical model of Beeman et al. [47] where they have predicted downshift of G line with increase of sp^3 fraction. D line position, optical gap and sp^3 fraction show a common transition point at 400℃ HTT (Figs. 3.11 and 3.14). Optical gap is almost stable and sp^3 fraction changed a little while D line shifts towards higher frequency due to HT upto 400℃ and above which, both optical gap and sp^3 fraction decrease rapidly while D line shifts towards lower frequency. Since optical gap remains constant and change of sp^3 fraction is very little upto 400℃, there is less possibility of change in bonding though D line shift is observed. We suggest this upshift of D line is due to the decrease of bond-angle disorder rather than the structural rearrangements through change in bonding. At higher HTTs, both optical gap and sp^3 fraction decrease rapidly (Fig. 3.14) which indicate downshift of D line towards 1355 cm^{-1} (Fig. 3.11) is mainly due to the change in bonding of the films, though the contributions due to bond angle disorder cannot be ruled out. The possible evolution of hydrogen might be the key to the structural changes above 400℃. The downshift of D line up to 1355 cm^{-1} reveals increasing dominance of crystallites and is confirmed by decrease of the FWHM of G and D lines (Fig. 3.12). At 800℃ HTT, position of G and D lines are about 1590 and 1355 cm^{-1} respectively which are characteristics of polycrystalline graphite—nano graphitic particles formed relatively at high HTTs.

3.3.2.2 Conclusions

The carbon thin films deposited at room temperature by ion beam sputtering are observed to be amorphous in nature from Raman scattering studies. Effect of heat treatment of the carbon films at various temperatures on the structural properties is determined through

Raman scattering analysis. The spectra were deconvoluted into D and G bands and the structural parameters are determined. The broad spectra along with the position of G peak at 1545 cm^{-1} (downshift from single crystal graphitic peak, 1580 cm^{-1}) of as-deposited film reveals amorphous nature of the film and has both trihedral and tetrahedral bonds in its structure. The upshift of G peak towards 1590 cm^{-1} shows evidence of a progressive formation of crystallites in carbon films upon heat treatment. Upshift and downshift of D line have been observed and we have related the former to the decrease of the bond-angle disorder and the latter mainly due to the decrease of the tetrahedral bonding in its structure.

References

[1] K. Yamamoto, Y. Koga, S. Fujiwara and F. Kokai: Jpn. J. Appl. Phys. 36 (1997) L1333.

[2] H. J. Scheibe and B. Schultrich: Thin Solid Films 246 (1994) 92.

[3] D. T. Peeler and P. T. Murray: Diamond & Relat. Mater. 3 (1994) 1124.

[4] F. Y. Chuang and C. Y. Sun: Appl. Phys. Lett. 69 (1996) 3504.

[5] J. U. Oh, K-R Lee and K. Y Eun: Thin Solid Films 270 (1995) 173.

[6] V. Palshin, E. I. Meletis, S. Ves and S. Logothetidis: Thin Solid Films 270 (1995) 165.

[7] M. Vogel, O. Stenzel, R. Petrich, G. Schaarschmidt and W. Scharff: Thin Solid Films 227 (1993) 74.

[8] N. Savvides and B. Window: J. Vac. Sci. & Technol. A 3 (1985) 2386.

[9] H. A. Yu, Y. Kaneko, S. Yoshimura and S. Otani: Appl. Phys. Lett. 68 (1996) 547.

[10] M. Uchida, H. Tanaka and K. Kotera: Jpn. J. Appl. Phys. 35 (1996) 5815.

[11] B. Dischler, A. Bubenzer and P. Koidl: Appl. Phys. Lett. 42 (1983) 636.

[12] Rusli, G. A. J. Amaratunga and S. R. P. Silva: Thin Solid Films 270 (1995) 160.

[13] J. Robertson: J. Non-Cryst. Solids 164-166 (1993) 1115.

[14] M. Matsuoka and K. Ono: Appl. Phys. Lett. 50 (1987) 1864.

[15] S. Matsuo and M. Kiuchi: Jpn. J. Appl. Phys. 22 (1983) L210.

[16] Y. H. Shing and F. S. Pool: Vacuum 41 (1990) 1368.

[17] B. Dischler, A. Bubenzer and P. Koidl: Solid State Commun. 48 (1983) 105.

[18] J. Besold, R. Thielsch, N. Matz, C. Frenzel, R. Born and A Mobius: Thin Solid Films 293 (1997) 96.

[19] J. J. Hauser: J. Non-Cryst. Solids 23 (1977) 21.

[20] M. Morgan: Thin Solid Films 7 (1971) 313.

[21] K. Mukhopadhyay, K. M. Krishna and M. Sharon: Phys. Rev. Lett. 72 (1994) 3182.

[22] M. Sharon, K. Mukhopadhyay, I. Mukhopadhyay and K. M. Krishna: Carbon 33 (1995) 331.

[23] K. Mukhopadhyay, K. M. Krishna and M. Sharon: Carbon 34 (1996) 251.

[24] K. Mukhopadhyay, K. M. Krishna and M. Sharon: Mat. Chem. & Phys. 49 (1997) 252.

[25] K. M. Krishna, T. Soga, K. Mukhopadhyay, M. Sharon and M. Umeno: Sol. Energy Mater. & Sol. Cells 48 (1997) 25.

[26] K. Chakrabarti, R. Chakrabarti, K. K. Chattopadhyay, S. Chaudhuri and A. K. Pal: Diamond & Relat. Mater. 7 (1998) 845.

[27] J. Tauc: Amorphous and Liquid Semiconductors (Plenum Press, London, New York, 1974) Chap.4.

[28] C. Wyon, R. Gillet and L. Lombard: Thin Solid Films 122 (1984) 203.

[29] E. A. Davis and N. F. Mott: Philos. Mag. 22 (1970) 903.

[30] A. Helmbold, P. Hammer, J. U. Thiele, K. Rohwer and D. Meissner: Philos. Mag. B 72 (1995) 335.

[31] L. Vescan, M. Telnic and C. Popescu: Phys. Status Solidi B 54 (1972) 733.

[32] S. Orzeszko, W. Bala, K. Fabisiak and F. Rozploch: Phys. Status Solidi 81 (1984) 579.

[33] S. M. Mominuzzaman, K. M. Krishna, T. Soga, T. Jimbo and M. Umeno: Carbon 38 (2000) 127.

[34] D. A. Anderson: Philos. Mag. 35 (1977) 17.

[35] G. Desrousseaux, A. Carlan and R. Faure: Thin Solid Films 76 (1981) 208.

[36] B. I. Shklovskii and A. L. Efros: Electronic Properties of Doped Semiconductors (Springer-Verlag, Berlin, 1984) p. 208.

[37] F. W. Smith: J. Appl. Phys. 55 (1984) 764.

[38] D. S. Knight, W. B.White, J. Mater. Res. 4 (1989) 385.

[39] M. S. Dresselhaus, G. Dresselhaus, P. C. Eklund, Science of fullerenes and carbon nanotubes. Academ ic:San Diego.1996:15-54.

[40] S. R. P. Silva, J. Robertson, G. A. J. Amaratunga, B. Rafferty, L. M. Brown, J. Schwan, D. F. Franceschini, G. Mariotto, J. Appl. Phys. 81(1997) 2626.

[41] P. Lespade, R. Al-Jishi, M. S. Dresselhaus, Carbon 20 (1982) 427.

[42] H. C. Tsai, D. B. Bogy, M. K. Kundmann, D. K. Veirs, M. R. Hilton, S. T. Meyer, J. Vac. Sci. & Technol A 6 (1988) 2307.

[43] A. Richter, H. J. Scheibe, W. Pompe, K.W. Brzezinka, I. Muhling J. Non-Cryst. Solids 88 (1986) 131.

[44] R. P. Vidano, D. B. Fischbach, Solid State Commun. 39 (1981) 341.

[45] M. Yoshikawa, N. Nagai, M. Matsuki, H. Fukuda, G.Katagiri, H. Ishida, A.Ishitani. Phys. Rev. B 46 (1992) 7169.

[46] R. O. Dillon, J. A. Woollam, V. Katkanant, Phys Rev B 29 (1984) 3482.

[47] D. Beeman, J. Silverman, R. Lynds, M.R. Anderson, Phys Rev B 30 (1984) 870.

[48] M. A. Tamor, W.C.Vasell, J Appl Phys 76 (1994) 3823.

[49] M. H. Grimsditch, A. K. Ramdas, Phys Rev B 11 (1975) 3139.

[50] F. Tuinstra, J. L. Koenig, J. Chem Phys 53 (1970) 1126.

[51] R. J. Nemanich, G. Lucovsky, Solid State Commun 23 (1977) 117.

[52] V. Meenakshi, A. Sayeed, S. V. Subramanyam, Mater Sci Forum 223-224 (1996) 307.

[53] M. Sharon, K. Mukhopadhyay, K. Yase, S. Iijima, Y. Ando, X. Zhao. Carbon 36 (1998) 507.

[54] K. M. Krishna, T. Soga, T. Jimbo and M. Umeno, Carbon 37 (1999) 531.

[55] S. T. Jackson, R. G. Nuzzo, Appl Surf Sci 90(1995) 195.

[56] Y. G. Gogotsi, M. Yoshimura, Nature 367(1994) 628.

[57] E. H. Lee, J. D. M. Hembree, G. R. Rao, L. K. Mansur, Phys Rev B 48 (1993-I) 15540.

[58] F. Richter, K. Bewilogua, H. Kupfer, I. Muhling, B. Rau, B. Rother, D. Schumacher, Thin Solid Films 212 (1992) 245.

[59] B.Dorfman, M. Abraizov, F.H. Pollak, D. Yan, M. Strngin, X. Q. Yang, Z. Y..Rong, Mater. Res. Soc. Symp. Proc. 349 (1994) 547.

[60] J. Robertson, Prog Solid St. Chem. 21(1991) 199.